Regular Article

PHYSICAL CHEMISTRY RESEARCH
Published by the
Iranian Chemical Society
www.physchemres.org
info@physchemres.org

Phys. Chem. Res., Vol. 9, No. 4, 637-649, December 2021
DOI: 10.22036/pcr.2021.276639.1898

Modified Mesoporous HMS Supported V/W for Oxidative Desulfurization of Dibenzothiophene

N. Jamali, N. Ramezani and M.H. Mousazadeh*

Department of Chemistry, Amirkabir University of Technology, 15875-4413, Tehran, Iran

(Received 17 March 2021, Accepted 2 July 2021)

This study examines the synthesis of two V/W-HMS (hexagonal mesoporous silica) compounds with various vanadium and tungsten loadings and their catalytic activities for oxidative desulfurization of dibenzothiophene (DBT) in the model diesel fuel. X-ray powder diffraction (XRD), scanning electron microscopy (SEM), Fourier transform infrared (FT-IR) spectroscopy and N_2 physical adsorption-desorption (BET/BJH) techniques were used to characterize these catalysts. According to our results, the best V/W-HMS catalyst exhibited high catalytic activity; it was capable of converting more than 95% of DBT in the model diesel fuel under the optimum reaction condition (0.05 g 1:4 of catalyst, T = 60 °C, t = 2 h). Doping of vanadium and tungsten led to a decrease in bandgap of the catalyst and an effective improvement in its catalytic performance. The catalytic activity remained unchanged even after 6 recycling processes. The reaction kinetics, mechanisms and bandgap energies of the catalysts were also investigated.

Keywords: Catalyst, Hexagonal mesoporous silica, Vanadium, Tungsten, DBT

INTRODUCTION

Commercial fuels include many sulfur-containing compounds which are converting into SO_x species during the combustion process in vehicle engines. These species cause acid rain, corrosion of equipment, catalyst poisoning, and other effects that lead to environmental pollution [1,2]. Recently, strict environmental regulations have been imposed by the governments for reducing the sulfur content of the diesel fuels used in vehicles, from 2000 to less than 10ppm; even greater reduction in sulfur content has been reported [3-5]. A traditional technique for desulfurization in petroleum industry is the hydrodesulfurization process (HDS) [6]. The HDS has some advantages, such as high efficiency and short reaction time. However, reducing the sulfur content of the commercial fuels to less than 10 ppm using HDS technique requires severe reaction conditions such as high-pressure hydrogen and high operating temperatures [4,7]. Hence, finding a new alternative method is of great interest. Recently, the oxidative desulfurization process (ODS) has been under the spotlight, and it has been investigated extensively due to its moderate reaction condition, high efficiency, lower investment requirements and its low process cost [8,9].

Since the structural properties of supports can affect the dispersion, stability and contacts of the active sites of catalyst with reactants, it can significantly influence the final rate of the process [10], and thus the selection of base structure is of great importance. Among the various solid supports, mesoporous silica with different structures such as MCM-41, SBA-15 and HMS attracted much attention due to their structural properties, uniform pore size distribution, high surface areas, and large pore volumes. Comparing with MCM-41 and SBA-15, HMS has higher chemical and thermal stability, shorter channels and better textural mesoporosity. This can provide better mass transfer channels for reactants to access the active sites of the catalyst [11,12]. Furthermore, to increase the surface acidity, the silicate framework of HMS materials can be modified with transition metals such as V, Ti, Fe, Cr, Co,

*Corresponding authors. E-mail: mousazadeh@aut.ac.ir

Cu, *etc*. [13-18]. This modification results in more diverse applications and improves the catalysts' activity. In this regard, several studies have been done on modified mesoporous materials and their applications have been investigated in the ODS process, *e.g.* $CoMoW/Al_2O_3$-TiO_2 (HDS) [19], phosphotungstic acid/TiO_2 [20], Au/Ti-HMS [21], Zn-HMS [22], V-HMS [23], Fe/V-HMS [24], MoWFe catalyst [5] and HPW/Zr-HMS [26]. Bimetallic catalyst showed more promising performance than monometallic ones due to synergistic effects of the two metals. Embedding metals in HMS increases its dispersionand specific surface area, and also provides more active centers with small bandgap energy for easier reduction/oxidation reaction [24,26].

In the present work, synthesis and application of new V/W-HMS catalysts in the ODS process are reported. The catalysts were characterized using various techniques and applied in the ODS process of model diesel fuel using H_2O_2 as an oxidant. The influence of V and W loadings, reaction temperature, catalyst dosage and time of the reaction run on the conversion of the ODS process were investigated. Furthermore, the reaction kinetics, mechanisms and band gap structures of the catalysts were also investigated.

EXPERIMENTAL

Materials

All chemicals were used in their original forms and without any further purification. Tetraethyl Orthosilicate (TEOS ≥ 99%), Sodium Orthovanadate (Na_3VO_4, 99%), Sodium Tungstate dihydrate ($Na_2WO_4.2H_2O$, 99%), Ethanol (EtOH, ≥ 99.5%), dibenzothiophene (DBT, ≥ 98%), acetonitrile, and hydrogen peroxide (H_2O_2, 30 wt%) were all purchased from Merck. Dodecylamine (DA, 95%) was purchased from Fluka.

Catalyst Preparation

In a typical synthesis, 17.6 ml ethanol was added to 135 ml of distilled water (solution A). Then, 11.5 ml tetraethyl *ortho* silicate was added to a mixture of 0.00295 g Na_3VO_4 and 0.0189 g Na_3VO_4 (solution B). Solution B was added to solution A under vigorous stirring. Then, 1.85 g dodecylamine was added dropwise into the solution. After stirring for 24 h at 298 K, the formed solid was recovered, washed with distilled water, dried at 373 K for 6 h, and finally, calcined at 823 K for 12 h under airflow. The resultant sample was denoted as V/W-HMS (1:4), where 1:4 is the molar ratio of V/W and the molar ratio of Si/M = 650 (M = V + W).

The ODS Reaction

A solution of dibenzothiophene in acetonitrile was used as a model diesel fuel, containing 500 ppm of the DBT. In a typical run, the oxidative desulfurization reaction was performed in a double-necked 100 ml round-bottomed flask containing 10 ml of model fuel, 0.05 g of catalyst (V/W-HMS), 1 ml of H_2O_2 as oxidant (excess, $H_2O_2/S > 4$ was considered to activate the catalyst), coupled with a water bath with the desired temperature, and under vigorous stirring. The sulfur concentration of the model fuel was measured using gas chromatograph instrument (GC-FID Agilent 7890 b with a hp-5 column (30 m × 0.25 μm)). The removal percentage of the DBT was calculated using the following formula:

$$DBT\ (\%) = \left(\frac{B_0 - B_t}{B_0}\right) \times 100 \quad (1)$$

Where the B_0 is the initial concentration of sulfur (DBT) in the solution, and B_t is the sulfur concentration of the diesel fuel after reaction time (t).

Characterization

The crystallographic structure of the catalysts examined using powder X-ray diffraction (XRD) (Radiation: 1.5406 Cu, Generator: 40 KV, 40 mA, I_{max} = 1529). Surface and textural properties of the catalysts were examined using N_2 adsorption-desorption isotherm with a Quantachrome Nova 2 instrument at 77 K. specific surface areas, and pore size distributions of the catalysts were calculated using the BET/BJH method. Scanning electron microscopy (SEM) was used for studying the surface morphology and dimensions. Fourier transform spectroscopy was used for studying the chemical bonding of the samples, using the KBr pallet technique (1:300 mg, 400-4000 cm^{-1}). To study bandgap structure of active sites of the catalysts, photoluminescence spectra of the catalysts were obtained with a Pekin Elmer LS55 Fluorescence spectrometer

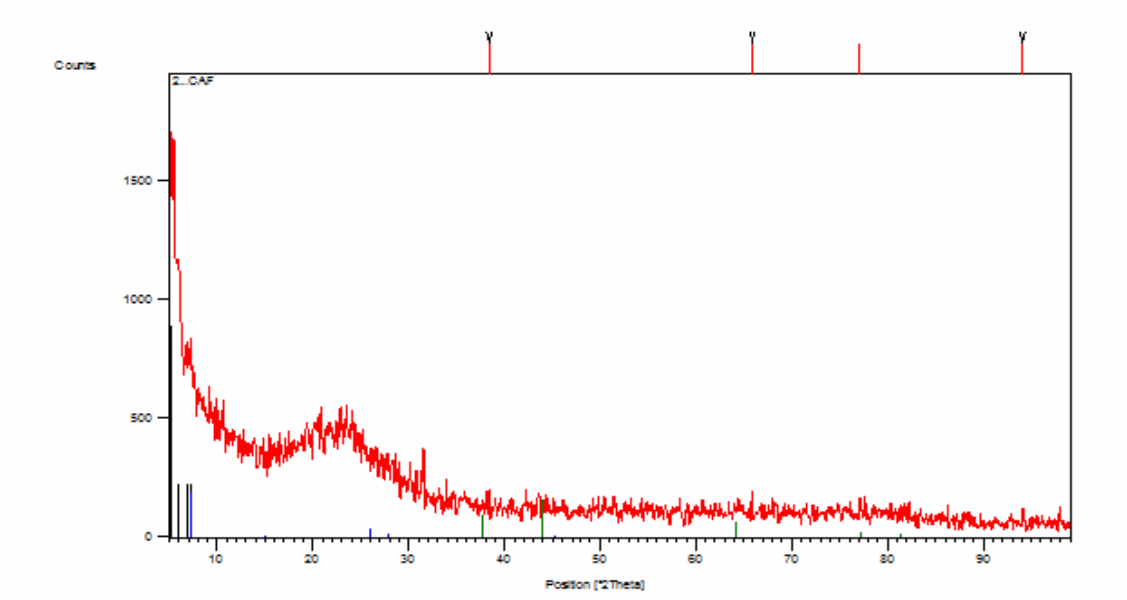

Fig. 1. Low and wide-angle XRD pattern of the V/W-HMS.

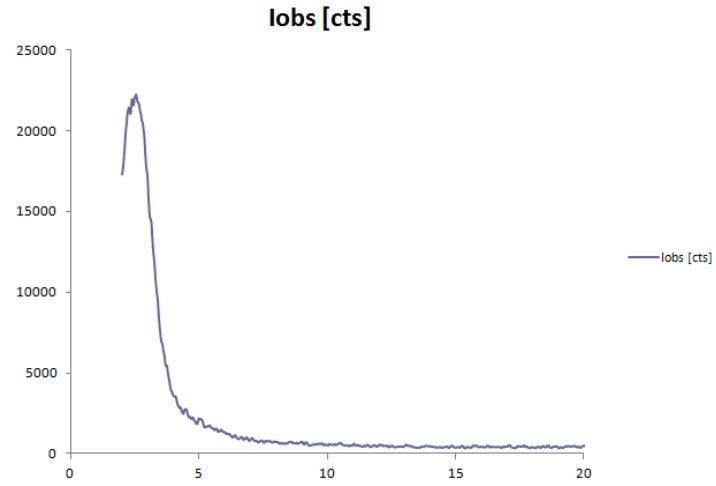

Fig. 2. XRD pattern of the pure HMS (low angel).

instrument. DRS spectra of the catalysts were also obtained with a Shimadzu diffuse reflectance spectrometer instrument, and the results were used for calculating the bandgap energy of the catalyst.

RESULTS AND DISCUSSION

Characterization of the Catalysts

The XRD patterns of V/W-HMS and pure HMS are presented in Figs. 1 and 2. Both samples exhibited typical diffraction peaks at $2\theta = 2.5$ that are associated with the HMS structures and indicate on successful synthesis of the hexagonal mesoporous structure. The peak of the V/W-HMS shifted to lower angles and became broader. These changes reveal that the unit cell parameters and d-spacing of V/W-HMS are more significant than those of pure HMS. Since the tungsten and vanadium were introduced into the silica lattice, and the Pauling radius of

W^{3+} (0.70 Å) or V^{4+} (0.58 Å) were higher than that of Si^{4+} (0.42 Å), these probably caused the lattice expansion and induced defects in the HMS structure [27,28].

With the incorporation of tungsten and vanadium, intensity of the diffraction peak was decreased, which probably caused by a disorder in mesoporous structure. Another possible reason for this phenomenon is the difference in the scattering constants between the pores and walls, and the formation of W and V nanostructures inside the channels of HMS [29]. The inflation of the wide-angle side of the XRD pattern is usually attributed to the defects in the HMS structure. The sample exhibited a broad peak at 2θ = 23°, which is typically ascribed to the characteristic peaks of the HMS framework with an amorphous feature. The several picks in the wide-angle side of the XRD pattern indicate the presence of aggregated clusters of vanadium and tungsten oxide species. The constant noise in the entire XRD pattern also confirms the presence of metal clusters with various sizes. As it is clear from the Figs. 1 and 2, the mesoporous structures have been successfully synthesized in both of the samples. The defects in structure of mesoporous silica in the sample containing metal oxides loaded on the base structure (Fig. 1), are probably due to the aggregation of vanadium and tungsten oxides species. This aggregation can deteriorate the mesoporous structure and cause defects in the HMS structure.

FT-IR spectra of the W/V-HMS sample, as-synthesized and recovered from one ODS process, are shown in Fig. 3. The absorption bands at 462, 805 and 1080 cm^{-1} are characteristics of the Si–O–Si vibrations [30]. The band at 960 cm^{-1} is attributed to the stretching vibration mode of a [SiO_4] unit bonded to the vanadium or tungsten species [31]. The results indicate the successful incorporation of vanadium and tungsten species into the silica framework. To further explore the effects of incorporating tungsten and vanadium in the HMS structure, N_2 adsorption-desorption isotherms of the samples were recorded. The adsorption-desorption isotherms and pore size distribution curves are shown in Figs. 4 and 5. All samples exhibited a type IV isotherm, which is the characteristic of the HMS structure. The quick pick of the BJH analysis confirms a uniform pore size distribution in all of the samples (Fig. 5). The small changes in the pore sizes are probably due to the differences in the size of the aggregated clusters of tungsten and vanadium. By increasing the amount of tungsten and decreasing the vanadium content, first in the (1:2) sample, the pore volume, pore size, and surface areas increased, which indicates a decrease in the size of the aggregated clusters. In the (1:3) sample, the pore size, volume and

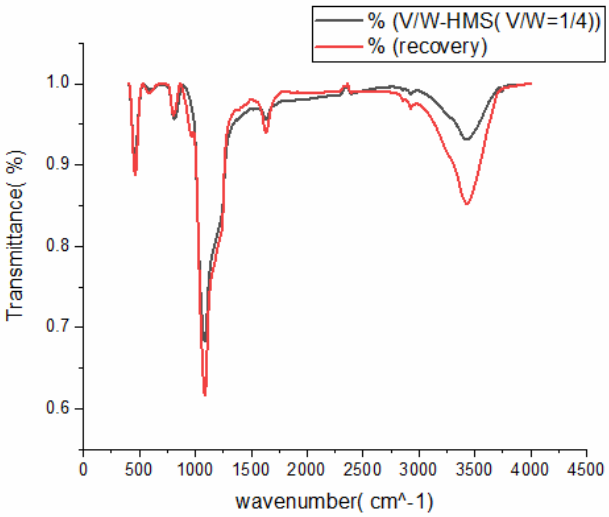

Fig. 3. FT-IR spectra of V/W-HMS (as-synthesized) and V/W-HMS (recovered).

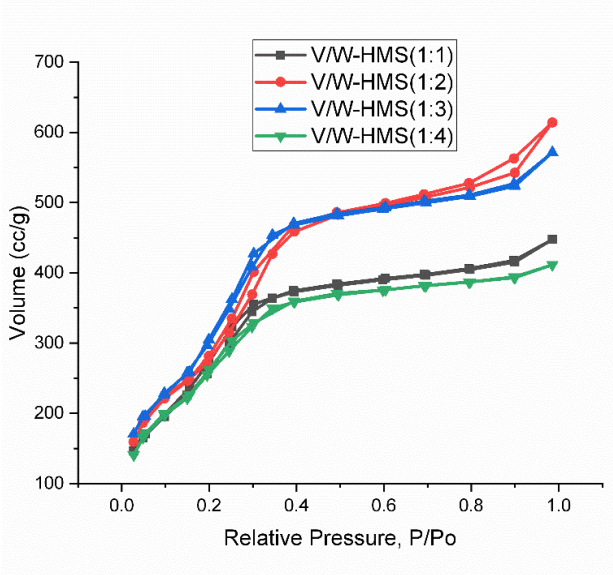

Fig. 4. The nitrogen adsorption-desorption isotherms of various V/W-HMS.

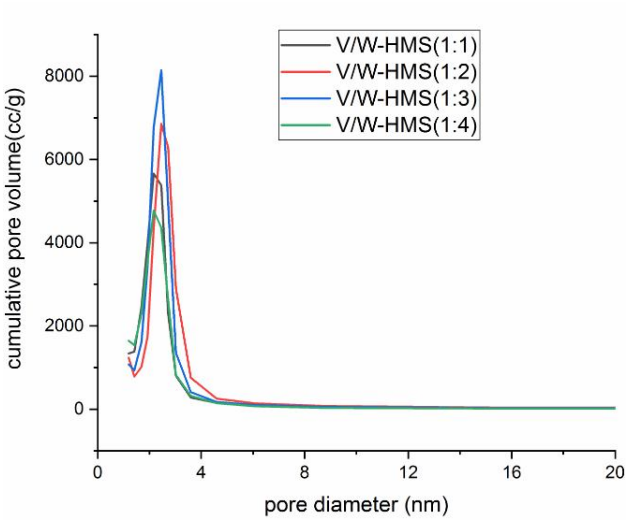

Fig. 5. BJH pore size distribution of various V/W-HMS.

surface area remained unchanged, which means that the size of the clusters did not change significantly.

Then, in the (1:4) sample, the pore size, volume, and surface area decreased again, which means that the cluster sizes increased again. These kinds of changes are probably due to some errors during the synthesis process. Detailed structural and surface properties of the catalysts are summarized in Table 1. The BET results show that the surface area, average pore size and volume of the HMS increased by adding V and W into the mesoporous structure of the HMS. The results suggest that the V and W are incorporated into the inner walls of the mesopores rather than inside the pores [32,33].

In addition, the size and morphology of the surface of catalyst were also investigated using SEM analysis.

Figures 6 and 7 show the surface of the pure HMS and the V/W-HMS catalyst. Comparison of the two images indicates that the vanadium and tungsten species have been successfully dispersed on the HMS structure.

Optimizing the ODS Reaction Condition

Effect of V/W content. The catalytic activity of obtained catalysts was studied with an oxidesulfurization process of the model diesel fuel. Scheme 1 shows a summary of the reaction. To find the optimum reaction conditions, first, the effect of various metal loadings (molar ratio of V:W, from 1:1 to 1:4) on the conversion of DBT was investigated. Other researches proved that the heavy loading of metal oxides on the base structures can lead to the aggregation of metal clusters, causing defects in the silica framework and reducing it catalytic activity. Besides, the practical application of a catalyst depends on the final price of its synthesis. Thus, reducing the amount of precious metal and substituting it with an abundant metal is of great interest. In Fig. 8, one can see the final conversion of the ODS reaction using catalysts with various W/V contents. As it is clear from Fig. 8, despite the reduction in the vanadium content, the catalysts with the molar ratio of V/W = 1:4 is still very effective in the ODS process.

Thus, it is reasonable to consider the V/W-HMS (1:4) as the optimum catalyst for the ODS reaction. It is worth mentioning that the overall loading of the metal oxides on the base structure in these catalysts is very low. These catalysts are 0.1 %wt with respect to their metal content (V + W). We calculated the catalysts' prices and compared them to each other. The 1:4 ratio catalyst was found to be significantly cheaper than the catalyst containing only vanadium.

Effect of the catalyst amount. The effect of the catalyst amount on the conversion of the ODS process was also studied for the catalyst dosages of 0.1, 0.05, 0.01 g (Fig. 9). It is clear that the conversion of the ODS process increases with an increase in the amount of catalyst in the reaction pot. Using 0.1 g of the catalyst can lead to more than 99% conversion. Result for sample containing 0.05 g of catalyst showed a lower conversion which indicates that the synthesis process was flawed and the dispersion of metal oxides was not good enough. However, since even 0.01 g of catalyst showed significant conversion, thus 0.05 g of catalyst was considered as the optimum catalyst dosage for the reaction.

Effect of oxidation temperature. Considering the V/W-HMS (1:4) as the best catalyst for the ODS process, the optimum reaction temperature for the ODS process was investigated, Fig. 10. As it is clear, the optimum temperature is 60 °C. It is worth mentioning that the conversion in 25 °C is very close to the conversion in 60 °C, which means that this catalyst is still effective even in low temperatures. This can be beneficial in terms of energy

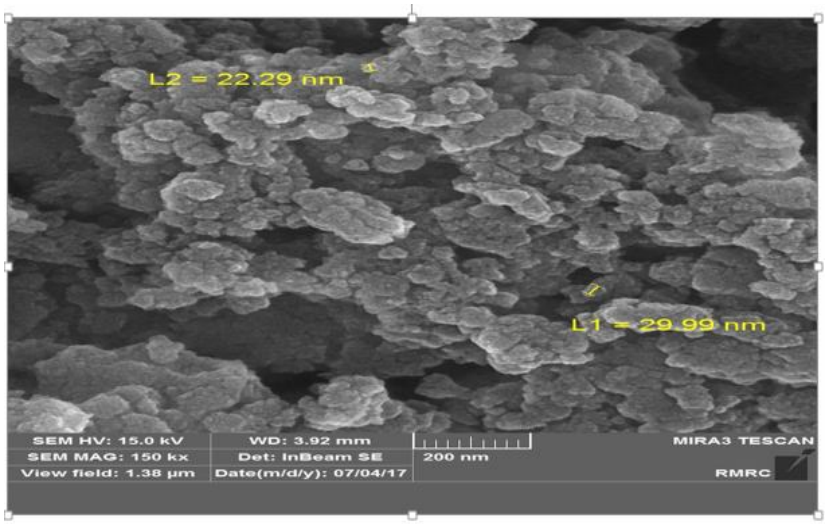

Fig. 6. SEM image of the pure HMS.

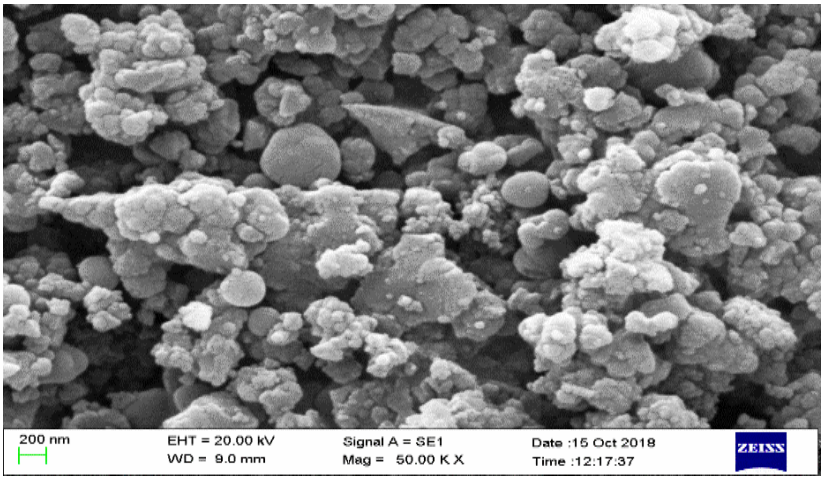

Fig. 7. SEM of the V/W-HMS.

Table 1. Textural and Structural Properties of the Synthesized Catalysts

Sample	SBET (m^2 g)	Pore volume (cc g^{-1})	Pore diameter (nm)
HMS	910	0.69	2.3
V/W-HMS(1/1)	1313	0.79	2.2
V/W-HMS(1/2)	1457	1.07	2.4
V/W-HMS(1/3)	1553	1.01	2.4
V/W-HMS(1/4)	1289	0.73	2.2

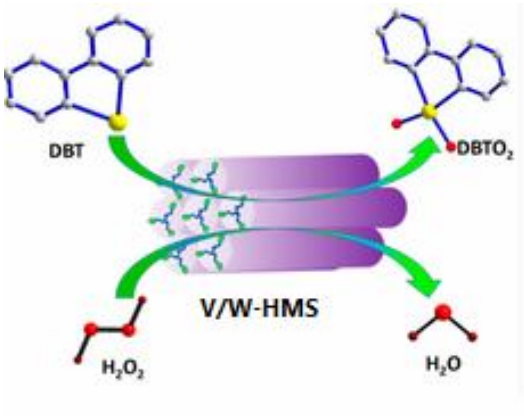

Scheme 1. Summary of the ODS process

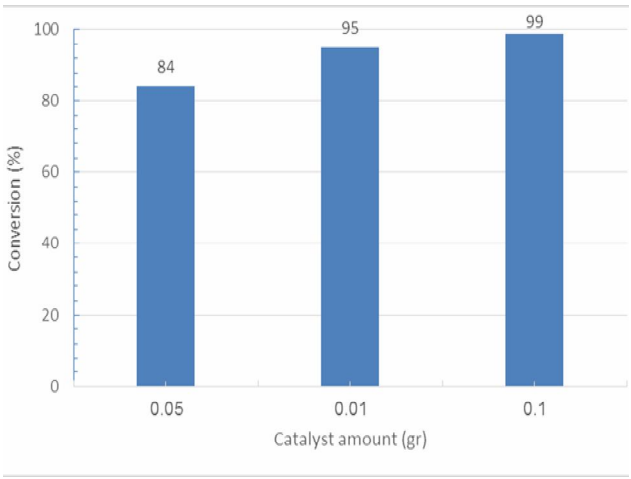

Fig. 9. Influence of different amounts of catalyst on the DBT removal. Reaction conditions: t = 2 h, H_2O_2 = 1.0 ml, T = 60 °C, 10.0 ml model fuel (DBT = 500 ppm), V/W-HMS (1:4).

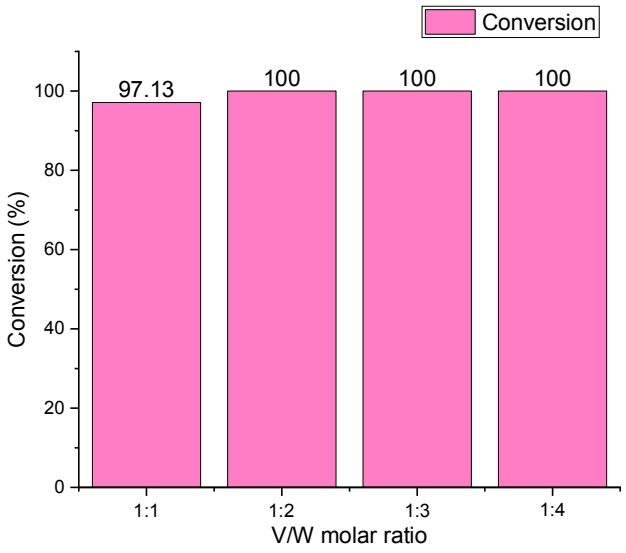

Fig. 8. Conversion of the ODS process using catalysts with different V/W ratio. Reaction conditions: T = 60 °C, t = 2 h, H_2O_2 = 1.0 ml, 10.0 ml model fuel (DBT = 500 ppm), catalyst = 1.0 g.

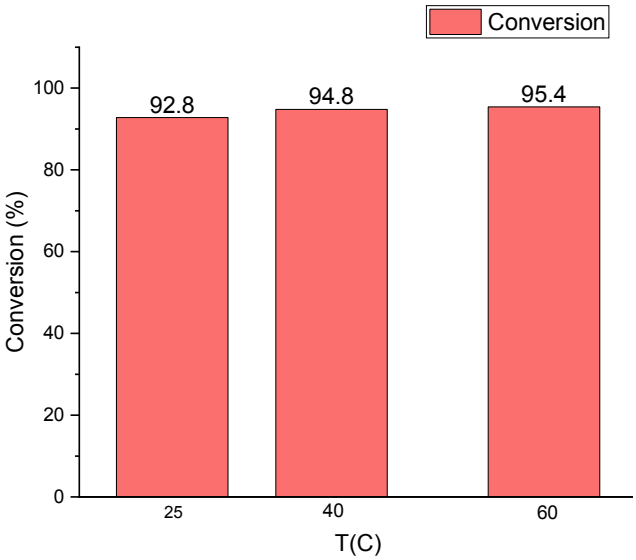

Fig. 10. Conversion of the ODS process in different temperatures. Reaction conditions: t = 2 h, H_2O_2 = 1.0 ml, 10.0 ml model fuel (DBT = 500 ppm), catalyst = 0.05 g V/W-HMS (1:4).

consumption. However, since better conversion was obtained at the 60 °C, this temperature was considered as the optimum reaction temperature.

The time of the reaction run. To find the optimum amount of time, the ODS process was performed with the V/W-HMS (1:4) catalyst, and real-time samples from the reaction solution were obtained and analyzed to determine its DBT concentration, Fig. 11. As it is clear, the optimum time of the reaction is 2 h or more, and a similar conversion cannot be obtained in lower reaction times.

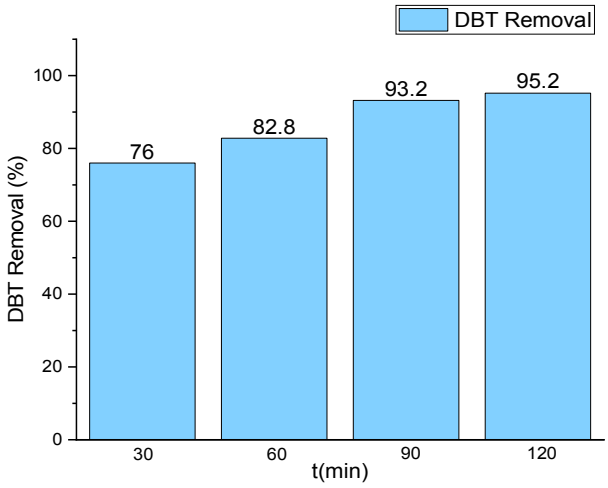

Fig. 11. Conversion of the ODS process in different times. Reaction conditions: t = 2 h, H_2O_2 = 1 ml, T = 60 °C 10 ml model fuel (DBT = 500 ppm), catalyst = 0.05 g V/W-HMS (1:4).

The Reaction Mechanism

Reaction mechanism is a key to elucidate the course of a reaction. The DBT oxidation takes place *via* a reaction between the DBT molecule and the active oxidative species generated by the reaction between the H_2O_2 and vanadium and tungsten oxides. The mechanisms of the metal-catalyzed oxidation reactions are classified into two types: Homolytic (radical) and Heterolytic (ionic) [4]. In the Heterolytic pathway, taking place over species such as WO_3, H_2O_2 reacts with the tungsten oxide species and generates inorganic peracids, the W-O-OH species (Scheme 2).

In the homolytic mechanism, the reaction of the H_2O_2 with the metal oxide species generates the $^{\bullet}OH$ free radical species (Eq. (1)). In the heterolytic mechanism, the oxidation state of the metal center does not change during the course of the reaction, while in the homolytic mechanism, it does. The homolytic mechanism requires cycling of the metal species between the two oxidation states. Thus, the homolytic mechanism is preferred due to easier reduction/oxidation of metal species.

$$M^{n+} + H_2O_2 \rightarrow M^{(n-1)+} + (^{\bullet}OOH + H^{+}) \quad (1)$$

$$M^{(n-1)+} + H_2O_2 \rightarrow M^{n+} + (^{\bullet}OH + {}^{-}OH) \quad (2)$$

$$(^{\bullet}OOH + {}^{\bullet}OH) \rightarrow H_2O + O_2 \quad (3)$$

Equation 1: Generation of the OH free radicals *via* the homolytic mechanism

According to the homolytic mechanism (Eq. (1)), the two essential steps are: (1) oxidation of intermediates by catalyst; and (2) reoxidation of the reduced catalyst. Step 1 requires an excellent oxidizing ability of the catalyst, and the rate of step 2 is determined by the reoxidability of the reduced molecule. The lowest unoccupied molecular orbital (LUMO)/highest occupied molecular orbital (HOMO) implies the ability of a molecule to accept/donate electrons. The lower the LUMO energy, the easier it is to accept electrons from H_2O_2. Therefore, the H_2O_2 adsorbing ability can be evaluated by LUMO. Step 1 has left the catalyst being reduced. Reoxidation of the reduced catalyst requires the reduced catalyst to donate its electrons easily to the oxidant. The higher the HOMO energy, the easier it is to donate electrons. Thus, the reoxidability can be evaluated by the HOMO energy of the reduced molecule (step 2). Easy reduction/oxidation is only possible if the energy states of the HOMO and LUMO orbitals are close together. Therefore, the reduction in bandgap energy can lead the entire process towards a homolytic mechanism. To study the presence of the hydroxyl radicals, a Terephthalic acid fluorescence approach was utilized [34,35]. In this method, the fluorescence intensity increases over time due to the reaction of $^{\bullet}OH$ radicals with the Terephthalic acid, Fig. 12. The linear increase in the intensity of the PL emission shows that a plethora of hydroxyl radicals are involved in the course of the reaction.

Electronic Structure

The properties of the V/W species depend upon their electronic structures. The structure of the molecular orbitals and the energy gap between the HOMO and LUMO orbitals significantly affect the activity and reaction mechanism. To study the bandgap energies of the catalyst, diffuse reflectance UV-Vis spectroscopy (DRS) and

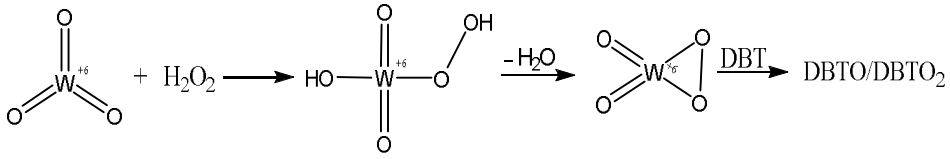

Scheme 2. The heterolytic reaction of the hydrogen peroxide and tungsten oxide species

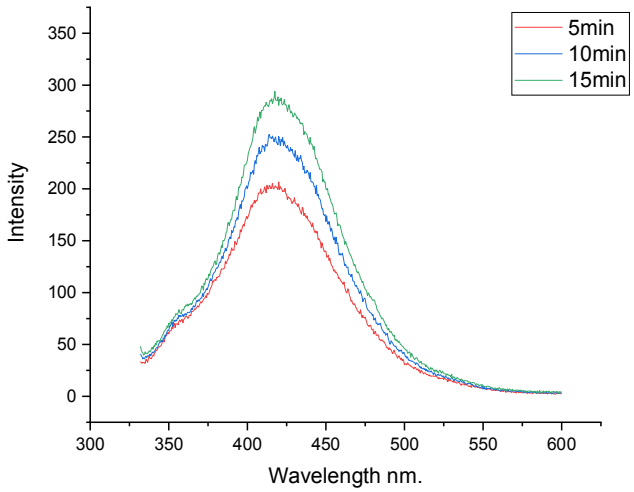

Fig. 12. Increase of the PL emission of the solution with time indicates the presence of the hydroxyl radicals. Reaction conditions: 0.05 g W/V-HMS (1:4), 1 ml H_2O_2, 20 ml Terephthalic acid solution 2 mM.

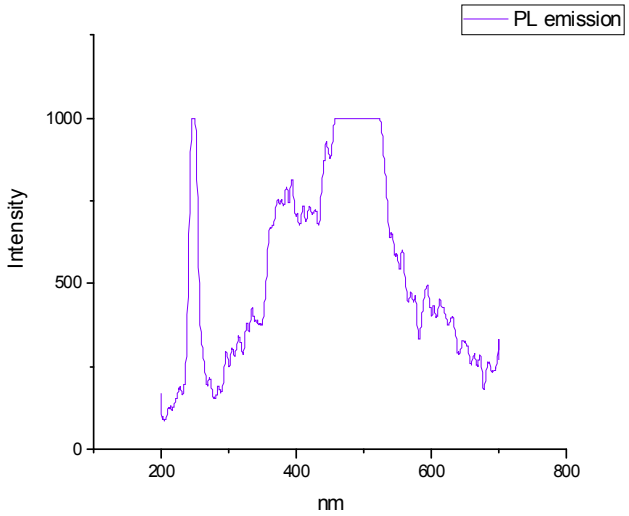

Fig. 13. Photoluminescence spectra of the W/V-HMS (1:4) Catalyst.

photoluminescence spectroscopy were used. To elucidate the bandgap structure of the catalysts, DRS and photoluminescence spectra of the catalysts were obtained using the following equation [36].

$$E^* = \frac{\lambda_{\max,abs} + \lambda_{\max,emis}}{\lambda_{intersect}}$$

In above equation, the E^* is the bandgap energy of the molecule, and $\lambda_{max.abs}$, $\lambda_{max.emis}$ and $\lambda_{intersect}$ can be obtained from the DRS/PL plot. $\lambda_{intersect}$ is the wavelength in which the DRS spectrum and PL spectrum intersect each other. Figures 13-15, show the PL/DRS spectra of the V/HMS and W/V-HMS. The two catalysts display significant emissions

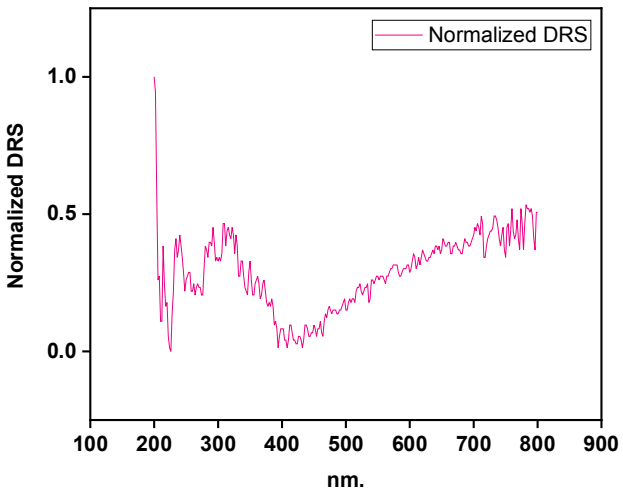

Fig. 14. DRS spectrum of the W/V-HMS (1:4) catalyst.

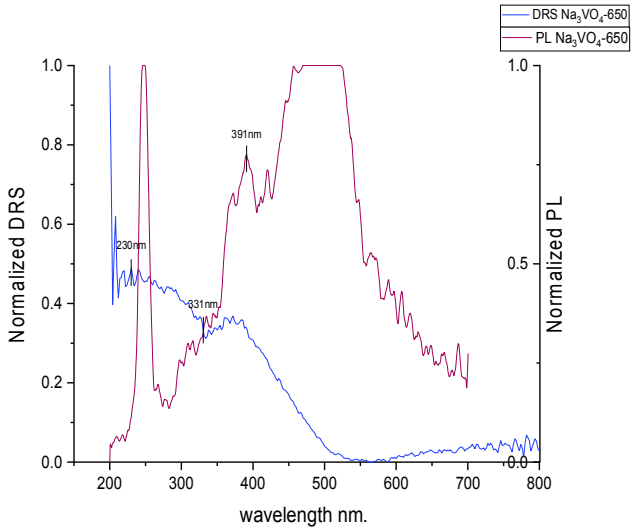

Fig. 15. Absorption (DRS)/emission (PL) spectra of the V/HMS (Na_3VO_4- 650, the Si/V ratio is 650).

that indicate the presence of significant optical bandgaps. Doping of the semiconductors, such as metal oxides (WO_4^{-2}), is a promising way to reduce the bandgap energies. The summary of the obtained bandgap structures can be found in Table 2. Since the bandgap energy for W/V-HMS is small, it means that the W-V species can easily undergo the reduction/oxidation process. The dominant reaction mechanism for the latter process is homolytic mechanism.

Kinetics of the ODS Reaction

The kinetics of the reaction was also investigated. Considering Fig. 16, one can conclude that the reaction kinetics is a pseudo-first-order reaction with the following rate equation:

$$\ln(C_t/C_0) = -kt$$

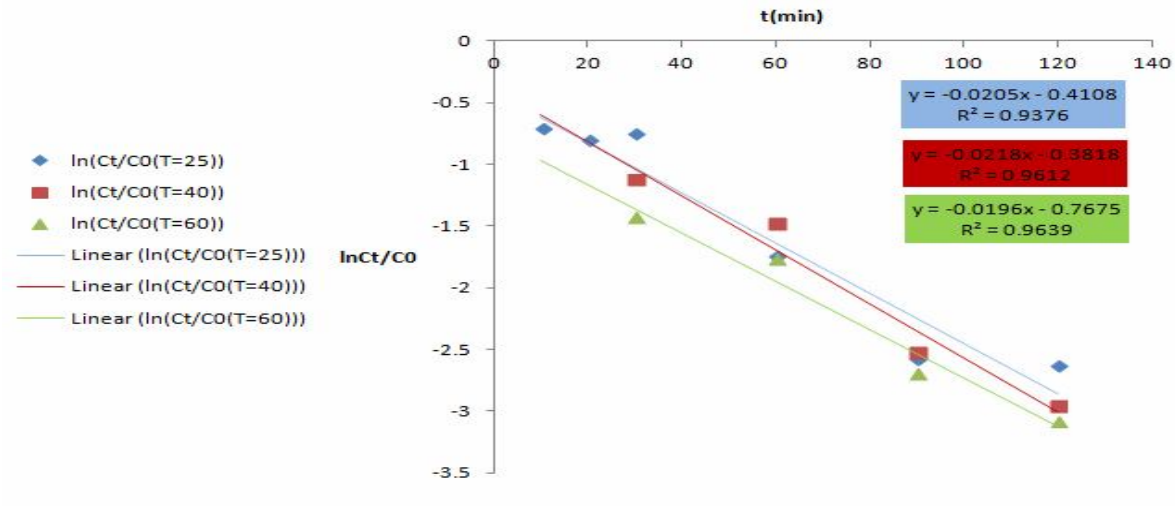

Fig. 16. First-order kinetic data at different temperatures.

Tables 2. Calculated Band Gaps of the Catalysts

Catalyst	$\lambda_{max.abs}$ (nm)	$\lambda_{max.ime}$ (nm)	$\lambda_{intersect}$ (nm)	Band gap (e v)
V/HMS	210	482	370	1.9
W/V-HMS	228	495	433	1.6

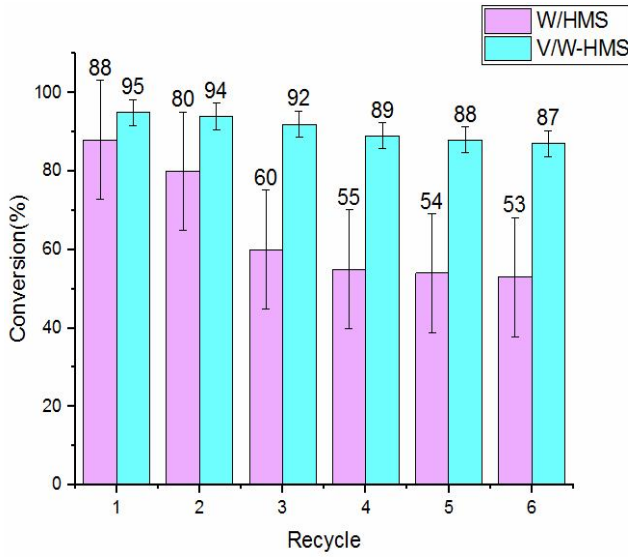

Fig. 17. The conversion of the ODS process, using the same catalyst after 6 reaction runs.

In above equation, the C_t is the concentration in time t, and C_0 is the initial concentration. The first-order kinetics of the reaction indicates the dominance of the homolytic pathway; no sign of a second mechanism was observed.

Reusability of the Catalyst

Finally, to investigate the chemical stability of the catalyst and the possibility of its recycling, 6 ODS reactions were performed. After each catalytic run, the catalyst was recovered by filtration, washed with methanol several times, and finally dried at 100 °C for 6 h. In every subsequent reaction run, performed in the presence of the recycled V/W-HMS catalyst, a slight reduction in the DBT conversion was observed (Fig. 17). However, the catalytic activity is fairly preserved even after six subsequent reaction runs. Slight leaching of active metal oxides is the most probable explanation for this phenomenon. Figure 17 also presents the DBT removal during the ODS process using W-HMS as catalysts in six subsequent runs. As it can be seen, the leaching of the W-HMS catalyst is significantly more than that of its W/V-HMS counterpart. This shows that the strong interactions between the V and W species suppress the leaching and deactivation of the catalyst. Thus, the V/W-HMS catalyst can be recycled and reused in subsequent reaction runs.

CONCLUSIONS

Tungsten and vanadium-containing mesoporous catalysts were prepared with various vanadium and tungsten loadings. The obtained catalysts were characterized, and their catalytic activities were investigated in the ODS process. W/V-HMS (1:4) proved to be an effective catalyst for the oxidative desulfurization of DBT in model diesel fuel. Under the optimum reaction conditions (T = 60 °C, t = 2 h, 1.0 ml H_2O_2, 0.05 g catalyst), the catalyst was capable of converting more than 95.4% of the DBT under mild reaction conditions. The mechanism of the reaction was studied, and the kinetics of the reaction was found to be a pseudo-first-order kinetics. The doping of vanadium and tungsten species reduced the bandgap of the catalyst and improved its catalytic performance. The catalyst was easily recycled and showed a stable performance after six cycles of regeneration.

ACKNOWLEDGMENTS

The author is interested in acknowledging the Amirkabir University of Technology (Tehran, Iran) for the financial support of this work. The authors thank Dr. H. Sid Kalal for providing XRD, SEM and BET analysis.

REFERENCES

[1] Capel-Sanchez, M. C.; Perez-Presas, P.; Campos-Martin, J. M.; Fierro, J. L. G., Highly efficient deep desulfurization of fuels by chemical oxidation. *Catal. Today* **2010**, *157*, 390-396, DOI: 10.1016/j.cattod.2010.01.047.

[2] Kayedi, N.; Samimi, A.; Asgari Bajgirani, M.; Bozorgian, A., Enhanced oxidative desulfurization of model fuel: A comprehensive experimental study. *S. Afr. J. Chem. Eng.* **2021**, *35*, 153-158, DOI: 10.1016/j.sajce.2020.09.001.

[3] Directive 2009/30/EC of the European parliament and of the council of 23 April 2009. *Offi. J. Eur. Union* **2018**, *55*, 88-113, DOI: 10.3000/17252555.L_2009.140.eng.

[4] Cao, Y.; Wang, H.; Ding, R.; Wang, L.; Liu, Z.; Lv, B., Highly efficient oxidative desulfurization of dibenzothiophene using Ni modified MoO_3 catalyst. *Appl. Catal. A: Gen*. **2020**, *589*, 117308-117348, DOI: 10.1016/j.apcata.2019.117308.

[5] Alvarez-Amparán, M. A.; Guillén-Aguilar, D.; Cedeño-Caero, L., MoWFe based catalysts to the oxidative desulfurization of refractory dibenzothiophene compounds: Fe promoting the catalytic performance. *Fuel Process. Technol.* **2020**, *198*, 106233-106242, DOI: 10.1016/j.fuproc.2019.106233.

[6] Qin, J. X.; Tan, P.; Jiang, Y.; Liu, X. Q.; He, Q. X.; Sun, L. B., Functionalization of metal-organic frameworks with cuprous sites using vapor-induced selective reduction: efficient adsorbents for deep desulfurization. *Green Chem.* **2016**, *18*, 3210-3215, DOI: 10.1039/C6GC00613B.

[7] Bakar, W. A. W. A.; Ali, R.; Kadir, A. A. A.; Mokhtar, W. N. A. W., Effect of transition metal oxides catalysts on oxidative desulfurization of model diesel. *Fuel Process. Technol.* **2012**, *101*, 78-84, DOI: 10.1016/j.fuproc.2012.04.004.

[8] Murata, S.; Murata, K.; Kidena, K.; Nomura, M., A novel oxidative desulfurization system for diesel fuels with molecular oxygen in the presence of cobalt catalysts and aldehydes. *Energ Fuels.* **2004**, *18*, 116-121, DOI: 10.1021/ef034001z.

[9] Ismagilov, Z.; Yashnik, S.; Kerzhentsev, M.; Parmon, V.; Bourane, A.; Al-Shahrani, F. M.; Hajji, A. A.; Koseoglu, O. R., Oxidative desulfurization of hydrocarbon fuels. *Catal. Rev.* **2011**, *53*, 199-255, DOI: 10.1080/01614940.2011.596426.

[10] Liu, D.; Zhou, W.; Wu, J., Effect of Ce and La on the activity of CuO/ZSM-5 and MnOx/ZSM-5 composites for elemental mercury removal at low temperature. *Fuel* **2017**, *194*, 115-122, DOI: 10.1016/j.fuel.2016.12.076.

[11] Du, S.; Li, F.; Sun, Q.; Wang, N.; Jia, M.; Yu, J., A green surfactant-assisted synthesis of hierarchical TS-1 zeolites with excellent catalytic properties for oxidative desulfurization. *Chem. Commu.* **2016**, *52*, 3368-3371, DOI: 10.1039/C5CC08441E.

[12] Tanev, P. T.; Pinnavaia, T. J., A neutral templating route to mesoporous molecular sieves. *Science* **1995**, *267*, 865-867, DOI: 10.1126/science.267.5199.865.

[13] Bazyari, A.; Khodadadi, A. A.; Mamaghani, H. A.; Beheshtian, J.; Thompson, L. T.; Mortazavi, Y., Microporous titania-silica nanocomposite catalyst-adsorbent for ultra-deep oxidative desulfurization. *Appl. Catal. B: Envir.* **2016**, *180*, 65-77, DOI: 10.1016/j.apcatb.2015.06.011.

[14] Liu, S.; Zhao, F.; Sun, H.; Liu, X.; Cui, B., Iron promotion of V-HMS mesoporous catalysts for ultra-deep oxidative desulfurization. *Appl. Organo. Chem.* **2018**, *32*, 1-9, DOI: 10.1002/aoc.4082.

[15] Long, Z.; Yang, C.; Zeng, G.; Peng, L.; Dai, C.; He, H., Catalytic oxidative desulfurization of dibenzothiophene using catalyst of tungsten supported on resin D152. *Fuel* **2014**, *130*, 19-24, DOI: 10.1016/j.fuel.2014.04.005.

[16] Rivoira, L. P.; Vallés, V. A.; Ledesma, B. C.; Ponte, M. V.; Martínez, M. L.; Anunziata, O. A., Sulfur elimination by oxidative desulfurization with titanium-modifiedSBA-16. *Catal.Today* **2016**, *271*, 102-113, DOI: 10.1016/j.cattod.2015.07.05.5.

[17] Safa, M. A.; Ma, X., Oxidation kinetics of dibenzothiophenes using cumene hydroperoxide as an oxidant over MoO_3/Al_2O_3. *Catal. Fuel* **2016**, *171*, 238-246, DOI: 10.1016/j.fuel.2015.12.050.

[18] Song, H. Y.; Li, G.; Wang, X. S.; Xu, Y. J., Characterization and catalytic performance of Au/Ti-HMS catalysts on the oxidative desulphurization using in situ H_2O_2: Effect of method catalysts preparation. *Catal. Today* **2010**, *149*, 127-131, DOI: 10.1016/j.cattod.2009.04.013.

[19] Obeso-Estrella, R.; Fierro, J. L. G.; Díaz de León, J. N.; Fuentes, S.; Alonso-Nuñez, G.; Lugo-Medina, E.; Pawelec, B.; Zepeda, T. A., Effect of partial Mo substitution by W on HDS activity using sulfide $CoMoW/Al_2O_3$-TiO_2 catalysts. *Fuel* **2018**, *233*, 644-657, DOI: 10.1016/j.fuel.2018.06.078.

[20] Yue, D.; Lei, J.; Peng, Y.; Li, J.; Du, X., Three-dimensional ordered phosphotungstic acid/TiO_2 with superior catalytic activity for oxidative desulfurization. *Fuel* **2018**, *226*, 148-155, DOI: 10.1016/j.fuel.2018.03.106.

[21] Song, H.; Li, G.; Wang, X.; Chen, Y., Characterization and catalytic performance of Au/Ti-HMS for direct generation of H_2O_2 and *in situ*-H_2O_2-

ODS from H_2 and O_2: An *in situ*-reduction synthesis and a recycle study of catalyst. *Micropor. Mesopor. Mater.* **2011**, *139*, 104-109, DOI: 10.1016/j.micromeso.2010.10.026.

[22] Wang, G. J.; Zeng, N., Preparation and catalytic properties of Zn-HMS molecular sieves. *Adv. Mater. Res.* **2012**, *560*, 300-304, DOI: 10.4028/www.scientific.net/AMR.560-561.300.

[23] Shiraishi, Y.; Naito, T.; Hirai, T., Vanadosilicate molecular sieve as a catalyst for oxidative desulfurization of light Oil. *Ind. Eng. Chem. Res.* **2003**, *42*, 6034-6039, DOI: 10.1021/ie030328b.

[24] FENG Su-Jiao, Y. B.; Yu, W.; Lin, Y.; Yong, H. H., Hydroxylation of benzene over V-HMS catalysts with the addition of Fe as the second metal component. *Acta Physico-Chimica Sinica*. **2011**, *27*, 2881-2886, DOI: 10.3866/pku.Whxb20112881.

[25] Wang, F.; Xiao, K.; Shi, L.; Bing, L.; Han, D.; Wang, G., Catalytic oxidative desulfurization of model fuel utilizing functionalized HMS catalysts: characterization, catalytic activity and mechanistic studies. *React. Chem. Eng.* **2021**, *6*, 289-297. DOI: 10.1039/D0RE00373E.

[26] Yuzbashi, S.; Mousazadeh, M. H.; Ramezani, N.; Sid Kalal, H.; Sabour, B., Mesoporous zirconium-silica nanocomposite modified with heteropoly tungstophosphoric acid catalyst for ultra-deep oxidative desulfurization. *Appl. Organ. Chem.* **2020**, *34*, e5326, DOI: 10.1002/aoc.5326.

[27] Zhang, Y.; Gao, F.; Wan, H.; Wu, C.; Kong, Y.; *et al.*, Synthesis, characterization of bimetallic Ce-Fe-SBA-15 and its catalytic performance in the phenol hydroxylation. *Micropor. Mesopor. Mater.* **2008**, *113*, 393-401, DOI: 10.1016/j.micromeso.2007.11.039.

[28] Kumar, D.; Pillai, K. T.; Sudersanan, V.; Dey, G. K.; Gupta, N. M., Hydrothermal synthesis and characterization of uranium-containing MCM-48 samples. *Chem. Mater.* **2003**, *15*, 3859-3865, DOI: 10.1021/cm030269s.

[29] Yang, C. M.; Liu, P. H.; Ho, Y. F.; Chiu, C. Y.; Chao, K. J., Highly dispersed metal nanoparticles in functionalized SBA-15. *Chem. Mater.* **2003**, *15*, 275-280, DOI: 10.1021/cm020822q.

[30] Sohn, J. R.; DeCanio, S. J.; Lunsford, J. H.; O'Donnell, D. J., Determination of framework aluminium content in dealuminated Y-type zeolites: a comparison based on unit cell size and wavenumber of IR bands. *Zeolites* **1986**, *6*, 225-227, DOI: 10.1016/0144-2449(86)90054-0.

[31] Chen, Y. W.; Lu, Y. H., Characteristics of V-MCM-41 and its catalytic properties in oxidation of benzene. *Ind. Eng. Chem. Res.* **1999**, *38*, 1893-1903, DOI: 10.1021/ie980665y.

[32] Wang, Z.; Xu, C.; Lu, Y.; Wu, F.; Ye, G.; Wei, G.; *et al.*, Visualization of adsorption: luminescent mesoporous silica-carbon dots composite for rapid and selective removal of U(VI) and in situ monitoring the adsorption behavior. *ACS Appl. Mater. Interfaces* **2017**, *9*, 7392-7398, DOI: 10.1021/acsami.6b13427.

[33] Wang, X.; Li, X.; Li, X; Wang, Y.; Han, Q.; *et al.*, Determination of 2,4,6-trinitrophenol by *in-situ* assembly of SBA-15 with multi-hydroxyl carbon dots. *Analy. Chimica Acta* **2020**, *1098*, 170-180, DOI: 10.1016/j.aca.2019.11.061.

[34] Bagheri, M.; Masoomi, M. Y.; Morsali, A., A MoO_3-Metal-organic framework composite as a simultaneous photocatalyst and catalyst in the PODS process of light oil. *ACS Catal.* **2017**, *7*, 6949-6956, DOI: 10.1021/acscatal.7b02581.

[35] Ishibashi, K. I.; Fujishima, A.; Watanabe, T.; Hashimoto, K., Detection of active oxidative species in TiO_2 photocatalysis using the fluorescence technique. *Electrochem. Commun.* **2000**, *2*, 207-210, DOI: 10.1016/S1388-2481(00)00006-0.

[36] Chen, K.; Zhang, X. M.; Yang, X. F.; Jiao, M. G.; Zhou, Z.; *et al.*, Electronic structure of heterojunction MoO_2/g-C_3N_4 catalyst for oxidative desulfurization. *Appl. Catalysis B: Envir.* **2018**, *238*, 263-273, DOI: 10.1016/j.apcatb.2018.07.037.